J. Fluid Mech. (1983), *vol.* 134, *pp.* 133–154
Printed in Great Britain

Flow between rotating disks. Part 2. Stability

By A. Z. SZERI, A. GIRON, S. J. SCHNEIDER†,
Department of Mechanical Engineering, The University of Pittsburgh, Pittsburgh, PA 15261
AND H. N. KAUFMAN
Research and Department Center, Westinghouse Electric Co., Beulah Rd, Pittsburgh PA 15235

(Received 3 June 1982)

Infinite-disk flows appear to possess multiple solutions at $E^{-1} = 275$ (Holodniok, Kubicek & Hlavacek 1977), where $E = \nu/s^2\omega$ is the Ekman number. One of these solutions exhibits characteristics of Couette flow and is stable in the circular domain $0 < r/s < 50$. The other two solutions, both Poiseuille-type flows, are unstable at all positions. The stable solution shows strong resemblance to experimental profiles obtained between finite disks. Stability of finite-disk flows is investigated in two cases: (i) one disk rotating and the other stationary, and (ii) counter-rotating disks. Photographs indicate presence of two instability types. Theoretical calculations are in fair agreement with experimental evidence on instability of type I.

1. Introduction

Although the study of stability of rotating-disk flows goes back some forty years, all investigations known to the authors are of flows bounded by a single rotating disk. Stuart (1955) examined stability at infinite Reynolds number and found good agreement with experimental data on the direction of wave propagation but overestimated the number of vortices. He then concluded that viscosity must have a considerable influence on the wavenumber. Brown (1961) extended Stuart's analysis by considering stability at finite Reynolds number. The basic flow equations contain curvature and Coriolis terms in the work of Kobayashi, Kohama & Takamadate (1980), but the axial velocity component as well as the inplane variation of the velocity are neglected. Szeri & Giron (1982) retain the axial velocity, in addition to terms considered by Kobayashi, and use an accurate spline expansion. Their results compare very favourably with the experimental data of Kobayashi.

Experimentally, Faller (1963) discovered two types of instabilities, named type I and type II, in the Ekman layer. The waves of each of these families form a series of horizontal roll vortices, whose spacing is related to the depth of the boundary layer. Others who studied these instabilities include Faller & Kaylor (1966), Tatro & Mollo-Christensen (1967), Caldwell & Van Atta (1970) and Weidman (1976). The Ekman velocity profiles exhibit numerous inflection points, each of which might give rise to instabilities. Faller & Kaylor (1966) found that the location of the type I vortices, which are stationary or nearly so, coincides with the first inflection point of the radial velocity. Stuart's (1955) analysis of inviscid instabilities of the flow on a single, infinite, rotating disk confirms this. In fact, Gregory, Stuart & Walker (1955) were truly the first to observe and calculate type I instabilities.

None of the single-disk stability studies referred to above mentioned an important discovery of recent years – multiplicity of the basic flow. The Kármán similarity transformation was shown by Batchelor (1951) to be applicable even when the fluid

† Also at Research and Development Center, Westinghouse Electric Co.

at infinity is rotating about the axis of the disk. Solutions have been obtained for various values of γ, the ratio of angular velocity at infinity to that of the disk, by Rogers & Lance (1960) and others. However, for values of γ in the range $-0.160 > \gamma > -1.4351$ it appeared to be impossible to find solutions. It is now clear that at $\gamma = -1.4351$ the solution of the equations becomes singular. At $\gamma = -0.160$ the situation was more mysterious. Weidman & Redekopp (1975) suggested singularity in this neighbourhood. The mystery was cleared up by Zandbergen & Dijkstra (1977) and by Dijkstra (1980), who showed that branching occurs at $\gamma = -0.16054$.

Multiplicity of basic flows, when the fluid is bounded by two infinite disks, has been reported even earlier. The original controversy is associated with the names of Batchelor (1951) and Stewartson (1953). Mellor, Chapple & Stokes (1968) produced several classes of solutions which are referred to as multiple-cell solutions. More recently, Nguyen, Ribault & Florent (1975) found both Batchelor-type and Stewartson-type solutions numerically, with the character of the flow depending on what starting values were assumed for the marching integration. Holodniok, Kubicek & Hlavacek (1977) identify as many as five solutions to the governing differential equations at a given (high) Reynolds number, two of which are of boundary-layer type. Their low-Reynolds-number solution is unique and the flow is of the Batchelor type, with a substantial portion of the fluid rotating as a rigid body. Additional solutions make their appearance as the Reynolds number is increased. Two of these solutions are of two-cell type, and there is a Stewartson-type solution exhibiting boundary layers on both disks. In a later paper Holodniok, Kubicek & Hlavacek (1981) use finite-difference discretization and Newton's method to demonstrate the existence of several additional branches of solution. However, they give detailed treatment only to the conditions $E^{-1} = 625$ and $\omega_1/\omega_2 = 0$, 1 and -1.

The purpose of the present research is to investigate which, if any, of the multiple solutions of infinite parallel disk flows (Holodniok *et al.* 1977) might be realizable in the laboratory. A necessary condition, though by no means sufficient, is that the flow be stable in some domain of parameter space. We also analyse finite-disk flows and show that the flow is least stable at the edge of the disk and near the centre of rotation.

2. Theoretical

The flow field is bounded by two parallel disks of infinite radii, located at $\bar{x}^3 = 0$ and $\bar{x}^3 = s$ respectively, in the cylindrical polar coordinate system $\{\bar{x}^1, \bar{x}^2, \bar{x}^3\}$. We define another orthogonal curvilinear coordinate system, the origin of which is located on the lower disk at $\bar{x}^1 = r$, some $\bar{x}^2$, via the transformation (Stuart 1955)

$$\mathrm{T}: \begin{cases} x^1 = r\left[\ln\left(\dfrac{\bar{x}^1}{r}\right)\cos\epsilon - (\bar{x}^2 + \Omega t)\sin\epsilon\right], \\ x^2 = r\left[\ln\left(\dfrac{\bar{x}^1}{r}\right)\sin\epsilon + (\bar{x}^2 + \Omega t)\cos\epsilon\right], \\ x^3 = \bar{x}^3. \end{cases} \tag{1}$$

Relative to the $\{x^i\}$, the physical components $\{U_x, V_y, W_z\}$ of the basic flow are given by

$$\begin{cases} U_x = \cos\epsilon\, U_r - \sin\epsilon(r\Omega - V_\theta), \\ V_y = \sin\epsilon\, U_r + \cos\epsilon(r\Omega - V_\theta), \\ W_z = W_z, \end{cases} \tag{2}$$

where $\{U_r, V_\theta, W_z\}$ is the flow velocity relative to $\{\bar{x}^i\}$.

In accordance with the linear theory of stability, the basic flow is perturbed by an infinitesimal wave. We look for instability to perturbation which propagates in the x^1 direction, the direction of least stability, with speed $\mathrm{Re}\,(\lambda/\alpha)$ relative to $\{x^i\}$ and a wavelength of $2\pi/\alpha$. Let $\{\boldsymbol{v}; p\}$ represent the perturbation, then

$$\{\boldsymbol{v}(x); p(x)\} = \{\boldsymbol{v}(x^3); p(x^3)\}\,\mathrm{e}^{\mathrm{i}(\alpha x^1 - \lambda t)}. \tag{3}$$

The linearized equations that govern the evolution of the perturbation are given by Greenspan (1968):

$$i\lambda\boldsymbol{v} + \boldsymbol{V}\cdot\operatorname{grad}\boldsymbol{v} + \boldsymbol{v}\cdot\operatorname{grad}\boldsymbol{V} + 2\boldsymbol{\Omega}\times\boldsymbol{v} = -\operatorname{grad}\frac{p}{\rho} + \nu\nabla^2\boldsymbol{v}, \tag{4a}$$

$$\operatorname{div}\boldsymbol{v} = 0. \tag{4b}$$

In addition to (4), we require the perturbation velocity to satisfy the conditions:

$$\boldsymbol{v}|_{x^3=0} = 0, \quad \boldsymbol{v}|_{x^3=s} = 0. \tag{4c}$$

The various dimensionless quantities employed in the analysis have the following definitions:

$$\left.\begin{aligned} &\{x^i\} = r\{x, y, \Delta z\}, \quad \{U_x, V_y, W_z\} = V_0\{\bar{U}_x, \bar{V}_y, \Delta\bar{W}_z\},\\ &Re = \frac{V_0 s}{\nu}, \quad \sigma = \frac{\alpha s}{h}, \quad c = \frac{\lambda h}{\alpha V_0}, \quad \Delta = \frac{s}{r}, \quad \delta = \frac{s}{hr},\\ &m_i = \frac{s}{h^2}\frac{\partial h}{\partial x^i}, \quad \Gamma_{ij} = \frac{s^2}{h^3}\frac{\partial^2 h}{\partial x^i\,\partial x^j}, \quad i,j = 1,2, \end{aligned}\right\} \tag{5}$$

and $V_0 = r\Omega$ is the local characteristic velocity. Upon decomposing (4a) along $\{x^i\}$ and substituting (5) into (4), the following set of equations results:

$$\begin{aligned} -\mathrm{i}\sigma c u - (m_1 v + \mathrm{i}\sigma v - m_2 u)\,V_y + \Delta\left(\frac{\mathrm{d}u}{\mathrm{d}z} - \mathrm{i}\sigma w\right)W_z - \left(m_1 V_y + \delta\frac{\partial V_y}{\partial x} - m_2 U_x - \delta\frac{\partial U_x}{\partial y}\right)v\\ + \left(\frac{\partial U_x}{\partial z} - \delta\Delta\frac{\partial W_z}{\partial x}\right)w + 2\Delta v = -\frac{1}{V_0}\delta\frac{\partial\bar{p}}{\partial x} - \frac{1}{Re}\Big[-\frac{\mathrm{d}^2u}{\mathrm{d}z^2} + \mathrm{i}\sigma\frac{\mathrm{d}w}{\mathrm{d}z} - (2m_1m_2 - \Gamma_{12}\\ + \mathrm{i}\sigma m_2)\,v + (2m_2^2 - \Gamma_{22})\,u\Big], \end{aligned} \tag{6a}$$

$$\begin{aligned} -\mathrm{i}\sigma c v + \Delta\frac{\mathrm{d}v}{\mathrm{d}z}W_z + (m_1 v + \mathrm{i}\sigma v - m_2 u)\,U_x + \frac{\partial V_y}{\partial z}w + \left(m_1 V_y + \delta\frac{\partial V_y}{\partial x} - m_2 U_x\right)u - 2\Delta u\\ = -\delta\frac{\partial V_y}{\partial y}v - \frac{1}{Re}\Big[-\frac{\mathrm{d}^2v}{\mathrm{d}z^2} + (2m_1^2 - \Gamma_{11} + \sigma^2)\,v + (\mathrm{i}\sigma m_2 - 2m_1m_2 + \Gamma_{12})\,u\Big], \end{aligned} \tag{6b}$$

$$\begin{aligned} -\mathrm{i}\sigma c w - \left(\frac{\mathrm{d}u}{\mathrm{d}z} - \mathrm{i}\sigma w\right)U_x - \frac{\partial v}{\partial z}V_y - \left(\frac{\partial U_x}{\partial z} - \delta\Delta\frac{\partial W_z}{\partial x}\right)u + \left(\delta\Delta\frac{\partial W_z}{\partial y} - \frac{\partial V_y}{\partial z}\right)v\\ = -\frac{1}{V_0}\frac{\partial\bar{p}}{\partial z} - \frac{1}{Re}\Big[\mathrm{i}\sigma\frac{\mathrm{d}u}{\mathrm{d}z} + \mathrm{i}\sigma m_1 w + \sigma^2 w + m_1\left(\frac{\mathrm{d}u}{\mathrm{d}z} - \mathrm{i}\sigma w\right) + m_1\frac{\mathrm{d}v}{\mathrm{d}z}\Big], \end{aligned} \tag{6c}$$

$$(m_1 + \mathrm{i}\sigma)\,u + m_2 v + \frac{\mathrm{d}w}{\mathrm{d}z} = 0. \tag{7}$$

Here we have dropped the bar that signifies a non-dimensional quantity.

Cross-differentiation eliminates the pressure, and substitution from the equation

of continuity (7) eliminates the velocity component u. The algebra is tedious and we give here only the final result:

$$\left(-m_2^2\frac{\partial V_y}{\partial z}-m_2\delta\frac{\partial^2 U_x}{\partial x\,\partial z}-2m_1^2\frac{\partial V_\theta}{\partial z}+m_1m_2\frac{\partial U_x}{\partial z}+m_1\delta\frac{\partial^2 U_x}{\partial z\,\partial y}\right.$$
$$-2i\sigma m_1\frac{\partial V_y}{\partial z}+i\sigma\delta\frac{\partial^2 U_x}{\partial z\,\partial y}\Big)v+\Big(i\sigma cm_2-m_2^2V_y-\Delta m_2\frac{\partial W_z}{\partial z}-m_2\delta\frac{\partial U_x}{\partial x}$$
$$-2V_ym_1^2+m_1m_2U_x+m_1\delta\frac{\partial U_x}{\partial y}+2\Delta m_1-2i\sigma m_1V_y$$
$$+i\sigma\delta\frac{\partial U_x}{\partial y}+2i\sigma\Delta\Big)\frac{dv}{dz}-\Delta m_2W_z\frac{d^2v}{dz^2}+\Big(m_1\frac{\partial^2U_x}{\partial z^2}-m_1\sigma^2c-m_1i\sigma\delta\frac{\partial W_z}{\partial x}+i\sigma m_1^2U_x$$
$$-i\sigma\Delta m_1\frac{\partial W_z}{\partial z}+i\sigma\frac{\partial^2U_x}{\partial z^2}-i\sigma^3c+\sigma^2\delta\frac{\partial U_x}{\partial x}+i\sigma^3U_x+\sigma^2\Delta\frac{\partial W_z}{\partial z}\Big)w$$
$$+\Big(-m_2\frac{\partial V_y}{\partial z}-\delta\frac{\partial^2U_x}{\partial x\,\partial z}-i\sigma\Delta m_1W_z+m_1\frac{\partial U_x}{\partial z}+\sigma^2\Delta W_z\Big)\frac{dw}{dz}$$
$$+\Big(i\sigma c-m_2V_\theta-\Delta\frac{\partial W_z}{\partial z}-\delta\frac{\partial U_x}{\partial x}-i\sigma U_x\Big)\frac{d^2w}{dz^2}-\Delta W_z\frac{d^3w}{dz^3}$$
$$=\frac{1}{Re}\Big[(2m_2^3-m_2\Gamma_{22}+2m_1^2m_2-\Gamma_{11}m_2+2i\sigma m_1m_2-\sigma^2m_2)\frac{dv}{dz}$$
$$-(2\sigma^2m_1^2+i\sigma^3m_1+\sigma^4)w+(2m_2^2-\Gamma_{22}+2\sigma^2+2m_1^2-\Gamma_{11}-i\sigma m_1)\frac{d^2w}{dz^2}$$
$$-m_2\frac{d^3v}{dz^3}-\frac{d^4w}{dz^4}\Big],\tag{8a}$$

$$\Big(m_1m_2V_y+\delta m_2\frac{\partial V_y}{\partial x}-2m_2^2U_x-2\Delta m_2+i\sigma cm_1-m_1^2U_x-2i\sigma m_1U_x$$
$$-\delta m_1\frac{\partial V_y}{\partial y}-\sigma^2c+\sigma^2U_x-i\sigma\delta\frac{\partial V_y}{\partial y}\Big)v+(-m_1\Delta W_z-i\sigma\Delta W_z)\frac{dv}{dz}$$
$$-\Big(m_1\frac{\partial V_y}{\partial z}+i\sigma\frac{\partial V_y}{\partial z}\Big)w+\Big(m_1V_y+\delta\frac{\partial V_y}{\partial x}-2m_2U_x-2\Delta\Big)\frac{dw}{dz}$$
$$=-\frac{1}{Re}\Big[(i\sigma m_2^2-2m_1m_2^2+\Gamma_{12}m_2-2m_1^3+\Gamma_{11}m_1-m_1\sigma^2-2i\sigma m_1^2$$
$$+i\sigma\Gamma_{11}-i\sigma^3)v+(m_1+i\sigma)\frac{d^2v}{dz^2}+(i\sigma m_2-2m_1m_2+\Gamma_{12})\frac{dw}{dz}\Big].\tag{8b}$$

(i) *Single disk*

The analysis was utilized to study the flow of a semi-infinite fluid bounded by a single disk (Szeri & Giron 1982). We put $s=\delta^*$, where δ^* is the displacement thickness, and applied the second boundary condition (4c) at $x^3\to\infty$. The ratio δ^*/r as well as the streamline curvatures m_1 and m_2 are of order Re^{-1} (Schlichting 1979); the governing equations were simplified by neglecting terms of order smaller than this, obtaining in the process Stuart's (1955) equations. The analysis retains the normal gradient of W_z in the boundary layer, and we find $R_c=8.0128\times10^4$, $n\approx26$ and $\epsilon=14°$ for the critical value of the Reynolds number $R=r^2\omega/\nu$, the number of vortices and the direction of least stability respectively. These are to be contrasted with the experimental data $R_c=8.8\times10^4$, $n=26$–33 and $\epsilon=13°$–$15°$ of Kobayashi *et al.* (1980).

(ii) *Parallel disks*

As s/r is no longer related to the Reynolds number, previous simplications of the equations are not available. Experimental evidence suggests, however, that $s/r < 10^{-1}$ and $Re > 10^3$, so that $\delta/Re < 10^{-4}$. Terms of this order or smaller were neglected. Thus the governing equations, shown below, contain additional terms not considered by Stuart (1955). They do simplify to Stuart's equation, however, under the proper conditions.

$$
\begin{aligned}
&(U_x-c)\left(\frac{\mathrm{d}^2w}{\mathrm{d}z^2}-\sigma^2w\right)-\frac{\partial^2U_x}{\partial z^2}w+\frac{\mathrm{i}}{\sigma Re}\left[\frac{\mathrm{d}^4w}{\mathrm{d}z^4}-2\sigma^2\frac{\mathrm{d}^2w}{\mathrm{d}z^2}+\sigma^4w\right]\\
&+\delta\left\{\left(2\frac{\partial V_y}{\partial z}\cos\epsilon-\frac{\partial U_x}{\partial z}\sin\epsilon\right)v+\left(2V_y\cos\epsilon-(U_x+c)\sin\epsilon-2\right)\frac{\mathrm{d}v}{\mathrm{d}z}\right.\\
&\left.-\frac{\mathrm{i}}{\sigma}\left(V_y\sin\epsilon\frac{\mathrm{d}^2w}{\mathrm{d}z^2}+\frac{\partial V_y}{\partial z}\sin\epsilon\frac{\mathrm{d}w}{\mathrm{d}z}+\frac{\partial}{\partial z}\left[W_z\left(\frac{\mathrm{d}^2w}{\mathrm{d}z^2}-\sigma^2w\right)\right]\right)\right\}\\
&+\delta\frac{\mathrm{i}}{\sigma}\left\{\left[\frac{\partial^2U_x}{\partial z^2}\cos\epsilon+(U_x-c)\sigma^2\cos\epsilon\right]w-U_x\cos\epsilon\frac{\mathrm{d}^2w}{\mathrm{d}z^2}\right\}+\delta^2\left\{\left(\frac{\partial W_z}{\partial z}+W_z\right)\cos\epsilon\,w\right\}\\
&-\frac{\mathrm{i}}{\sigma}\delta^2\left\{\left(\frac{\partial V_y}{\partial z}\sin^2\epsilon+2\frac{\partial V_y}{\partial z}\cos^2\epsilon-\frac{\partial U_x}{\partial z}\cos\epsilon\sin\epsilon\right)v\right.\\
&\left.+\left(V_y\sin^2\epsilon+2V_y\cos^2\epsilon-U_x\cos\epsilon\sin\epsilon+\frac{\partial W_z}{\partial z}\sin\epsilon-2\cos\epsilon\right)\frac{\mathrm{d}v}{\mathrm{d}z}+W_z\sin\epsilon\frac{\mathrm{d}^2v}{\mathrm{d}z^2}\right\}=0, \qquad (9a)
\end{aligned}
$$

$$
\begin{aligned}
&(U_x-c)v+\frac{\mathrm{i}}{\sigma Re}\left(\frac{\mathrm{d}^2v}{\mathrm{d}z^2}-\sigma^2v\right)-\frac{\mathrm{i}}{\sigma}\frac{\partial V_y}{\partial z}w+\delta\left\{-\frac{\mathrm{i}}{\sigma}\left[(U_x\cos\epsilon+V_y\sin\epsilon)v+W_z\frac{\mathrm{d}v}{\mathrm{d}z}\right]\right.\\
&\left.+\frac{2}{\sigma^2}(V_y\cos\epsilon-U_x\sin\epsilon-1)\frac{\mathrm{d}w}{\mathrm{d}z}\right\}-\frac{\mathrm{i}\delta}{\sigma}(U_x-c)\cos\epsilon\,v-\frac{\delta}{\sigma^2}\frac{\partial V_y}{\partial z}\cos\epsilon\,w\\
&+\frac{\delta^2}{\sigma^2}\left\{(-2U_x\sin^2\epsilon+V_y\sin\epsilon\cos\epsilon-2\sin\epsilon-U_x\cos^2\epsilon)v-W_z\cos^2\epsilon\frac{\mathrm{d}v}{\mathrm{d}z}\right\}=0. \qquad (9b)
\end{aligned}
$$

To arrive at (9*a*, *b*) the following approximations were made:

$$
\left.\begin{aligned}
&\delta\approx\Delta, \quad m_1\approx\delta\cos\epsilon, \quad m_2\approx\delta\sin\epsilon,\\
&\Gamma_{11}\approx\delta^2\cos^2\epsilon, \quad \Gamma_{12}\approx\delta^2\sin\epsilon\cos\epsilon, \quad \Gamma_{22}\approx\delta^2\sin^2\epsilon.
\end{aligned}\right\} \qquad (10)
$$

Making use of the von Kármán (1921) similarity transformation, we have

$$
U_x=r\Omega\phi(z); \quad V_y=r\Omega\Psi(z), \quad W_z=(\nu\Omega)^{\frac{1}{2}}H(z), \qquad (11a)
$$

where

$$
\left.\begin{aligned}
\phi(z)&=\cos\epsilon\,F(z)-\sin\epsilon\,(1-G(z)),\\
\Psi(z)&=\sin\epsilon\,F(z)+\cos\epsilon\,(1-G(z)).
\end{aligned}\right\} \qquad (11b)
$$

Here $\{F(z), G(z), H(z)\}$ represents the similarity solution of the basic flow problem (Holodniok *et al.* 1977). Thus from (11*a*, *b*) we have

$$\begin{Bmatrix} \dfrac{\partial}{\partial x} \\ \\ \dfrac{\partial}{\partial y} \end{Bmatrix} \{U_x, V_y\} = \begin{Bmatrix} \cos\epsilon \\ \\ \sin\epsilon \end{Bmatrix} \{U_x, V_y\}.$$

Since the velocity component u does not appear in these equations, the boundary conditions of (9*a*, *b*) are chosen as

$$v = w = \frac{\mathrm{d}w}{\mathrm{d}z} = 0 \quad (z = 0, 1), \tag{12}$$

in place of (4*c*). The condition $\mathrm{d}w/\mathrm{d}z = 0$ at $z = 0, 1$ is a derived condition; it is obtained from the equation of continuity (7).

The remainder of this paper is concerned with obtaining solutions of the system composed of (9*a*, *b*) and boundary conditions (12).

3. Numerical

We seek solutions of Eq. (9) in the weak form

$$\left.\begin{aligned} v(z) &= \sum_{i=1}^{N} v_i B_i(z), \\ w(z) &= \sum_{j=1}^{N} w_j B_j(z). \end{aligned}\right\} \tag{13}$$

Here the $B_i(z), 1 \leqslant i \leqslant N$ are cubic B-splines defined over the partition

$$\pi: 0 = z_1 < z_2 < \ldots < z_{l+1} = 1 \tag{14}$$

with uniform smoothness $\nu_i = \nu = 3, 2 \leqslant i \leqslant l$, on the interior breakpoints, and a knot sequence

$$\left.\begin{aligned} z_1 &= t_1 = t_2 = t_3 = t_4, \\ z_2 &= t_5, \\ &\vdots \\ z_l &= t_N, \\ z_{l+1} &= t_{N+1} = t_{N+2} = t_{N+3} = t_{N+4}. \end{aligned}\right\} \tag{15}$$

The B-splines have the following relevant properties (de Boor 1978):

$$\left.\begin{aligned} B_1(z_1) &= B_N(z_{l+1}) = 1, \\ B_j(z_1) &= 0 \quad (j > 1), \\ B_j(z_{l+1}) &= 0 \quad (j < N); \end{aligned}\right\} \tag{16a}$$

$$\left.\begin{aligned} B_j(z) &= 0 \quad (z \notin [t_j, t_{j+4}]), \\ B_j(z) &\geqslant 0 \quad (z \in [0, 1]); \end{aligned}\right\} \tag{16b}$$

$$\left.\begin{aligned} B_1'(z_1) &= -B_2'(z_1) \neq 0, \\ B_j'(z_1) &= 0 \quad (j > 2), \\ B_N'(z_{l+1}) &= -B_{N-1}'(z_{l+1}) \neq 0, \\ B_j'(z_{l+1}) &= 0 \quad (j < N-1). \end{aligned}\right\} \tag{16c}$$

The expansions (13) can be forced to satisfy the boundary conditions (12) in the strong form via the spline properties (16). This yields

$$v(z) = \sum_{i=2}^{N-1} v_i B_i(z), \quad w(z) = \sum_{j=3}^{N-2} w_j B_j(z). \tag{17a, b}$$

The approximations (17) are substituted into (9), together with spline expansions for the basic flow

$$U_x = \sum_{p=1}^{N} U_p B_p(z), \quad V_y = \sum_{s=1}^{N} V_s B_s(z), \quad W_z = \sum_{t=1}^{N} W_t B_t(z). \tag{18}$$

$\{U_x, V_y, W_z\}$ are available in the literature (see e.g. Holodniok *et al.* 1977).

In the application of Galerkin's method, the expansion (17) is substituted into (9*a*, *b*). The first of the resulting equations is multiplied through by elements of the test τ^w and the second equation by elements of τ^v:

$$\tau^w = \{B_i(z): 3 \leqslant i \leqslant N-2\}, \quad \tau^v = \{B_j(z): 2 \leqslant j \leqslant N-1\}. \tag{19}$$

Integration over the domain $0 \leqslant z \leqslant 1$ leads to the complex algebraic eigenvalue problem

$$|\boldsymbol{X} - c\boldsymbol{Y}| = 0. \tag{20}$$

The complex matrices $\boldsymbol{X}$ and $\boldsymbol{Y}$ are defined as follows:

$$\begin{aligned} \mathrm{Re}(\boldsymbol{X}) &= \begin{bmatrix} \boldsymbol{A} & \boldsymbol{B} \\ \boldsymbol{C} & \boldsymbol{D} \end{bmatrix}, \quad \mathrm{Im}(\boldsymbol{X}) = \begin{bmatrix} \boldsymbol{E} & \boldsymbol{F} \\ \boldsymbol{G} & \boldsymbol{Q} \end{bmatrix}, \\ \mathrm{Re}(\boldsymbol{Y}) &= \begin{bmatrix} \boldsymbol{H} & \boldsymbol{I} \\ \boldsymbol{J} & 0 \end{bmatrix}, \quad \mathrm{Im}(\boldsymbol{Y}) = \begin{bmatrix} 0 & \boldsymbol{M} \\ \boldsymbol{N} & 0 \end{bmatrix}. \end{aligned} \tag{21}$$

The real matrices $\boldsymbol{A}, \boldsymbol{B}, \ldots, \boldsymbol{Q}$ are given in the appendix.

The flow is marginally or neutrally stable if there is one eigenvalue with $\mathrm{Im}(c) = 0$ and $\mathrm{Im}(c) > 0$ for all other eigenvalues. It is unstable if at least one eigenvalue exists with $\mathrm{Im}(c) < 0$. The marginal state is steady if $\mathrm{Re}(c) = 0$, but as there is no justification to assume that the principle of exchange of stability holds (Kobayashi *et al.* 1980) $\mathrm{Re}(c) \neq 0$ is retained.

To investigate the accuracy of Galerkin's method with B-splines for stability calculations, we have performed numerical studies of plane Poiseuille flow (Szeri & Giron 1982). Equations (9*a*, *b*) are easily reducible to the Orr–Sommerfeld equation for pressure flow between parallel plates, and the stability of this flow has been studied extensively. Grosch & Salwen (1968) used expansions in the eigenfunctions of the operator $(\mathrm{d}^2/\mathrm{d}z^2 - \sigma^2)$, and at $Re = 20000$ and $\sigma = 2.0$ calculated the first eigenvalue as $c_1 = 0.237413 + 0.003681\mathrm{i}$, using an expansion involving up to 50 symmetric eigenmodes. Orszag (1971) employed Chebyshev-polynomial expansion and obtained $c_1 = 0.23752649 + 0.00373967\mathrm{i}$ on a CDC 6600 computer (15 significant digits in single precision.) Our result for $Re = 20000$ and $\sigma = 2.0$ is $c_1 = 0.237394 + 0.00373133\mathrm{i}$, obtained on the PDP-10 (8 significant digits in single precision).

Our result of $Re_c = 11537.09$ is in error only by -0.06% when compared with Orszag's result.

4. Results and discussion

In one of the most thorough discussions to date on the primary flow between infinite rotating disks, Holodniok *et al.* (1977, 1981) report unique basic motion at $E^{-1} = 100$. The velocity components of this flow, as obtained from Holodniok's paper, were projected onto directions inclined locally to the radius at the angle ϵ. The various velocity profiles $V_\epsilon = U_r \cos\epsilon + V_\theta \sin\epsilon$ obtained in this manner (figure 1), were then analysed for stability to infinitesimal disturbances, assumed to propagate in the direction characterized by ϵ. Figure 2 shows a plot of the Reynolds number obtained

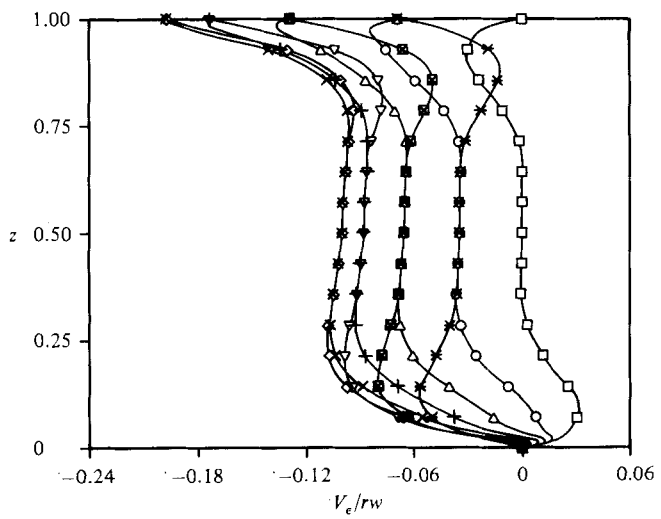

FIGURE 1. Directional behaviour of velocity (Holodniok *et al.* 1977); infinite disks, one disk rotating, $E^{-1} = 100$: □, $\epsilon = 0°$; ○, 20°; △, 40°; +, 60°; ×, 80°; ◇, 100°; ▽, 120°; ⊠, 140°; *, 160°.

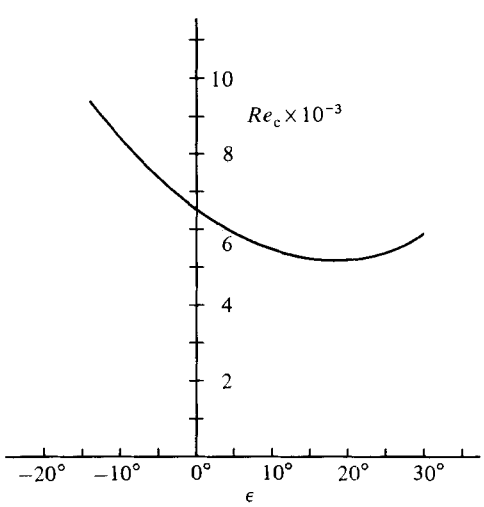

FIGURE 2. Directional behaviour of Reynolds number in marginal state; infinite disks, one disk rotating, $E^{-1} = 100$.

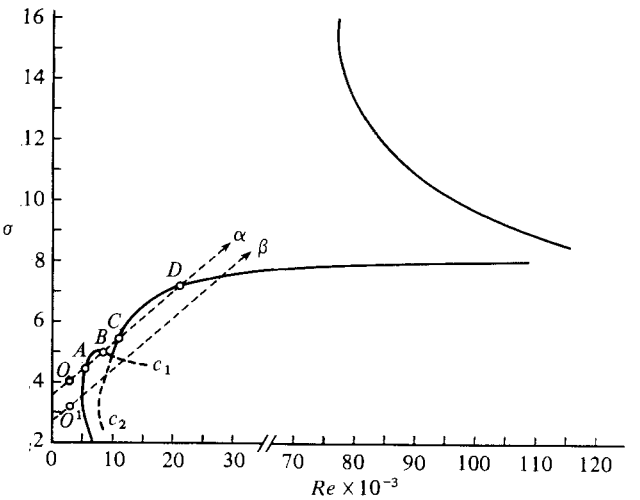

FIGURE 3. Diagram of neutral stability; infinite disks, one disk rotating, $E^{-1} = 100$, $\epsilon = 17°$.

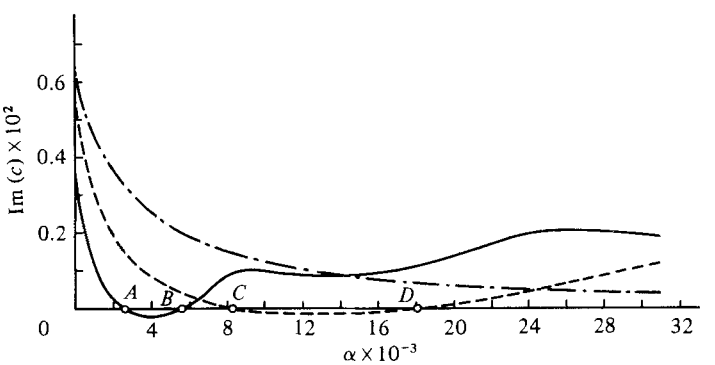

FIGURE 4. Variation of Im (c) along α; infinite disks, one disk rotating, $E^{-1} = 100$: –, Im (c_1); ––, Im (c_2); – –, Im (c_3).

at the marginal state of stability for a given profile versus the corresponding vortex angle ϵ, indicating that critical conditions occur at $17° < \epsilon < 20°$. The complete stability diagram for the flow is shown in figure 3.

When investigating Poiseuille flows or boundary-layer flows, the eigenvalues are found to retain their relative ordering over the whole parameter range (Grosh & Salwen 1968). They also vary continuously with the parameters; in consequence the contour representing marginal state of stability is smooth. None of this holds true in the case under consideration. The stability curve of figure 3 exhibits only piecewise smoothness.

Let the symbol α designate a contour in the $\{\sigma, Re\}$-space (figure 3). This contour has the equation $\sigma = 1.7243 \times 10^{-4} Re + 3.54$. Let the arclength along this contour, as measured from the point O, be α and let α_A, α_B, α_C and α_D designate arclengths OA, OB, OC and OD respectively. At $\alpha = 0$ all eigenvalues have positive imaginary part and the flow is stable to infinitesimal perturbations. Moving from O to the right along α, we encounter the point $A(\alpha_A)$ where the imaginary part of the first eigenvalue vanishes. (We labelled the eigenvalue that is dominant at this point in parameter space the first eigenvalue c_1.) At $\alpha = \alpha_A$, Im $(c_1) = 0$, Im $(c_k) > 0$, $k > 1$. For

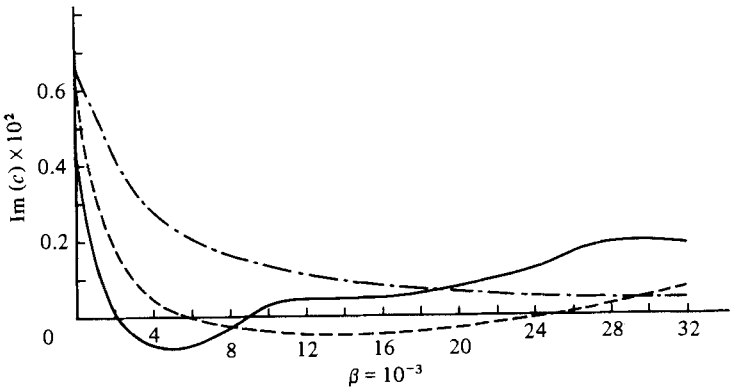

FIGURE 5. Variation of Im (c) along β; infinite disks, one disk rotating, $E^{-1} = 100$: –, Im (c_1); ——, Im (c_2); – –, Im (c_3).

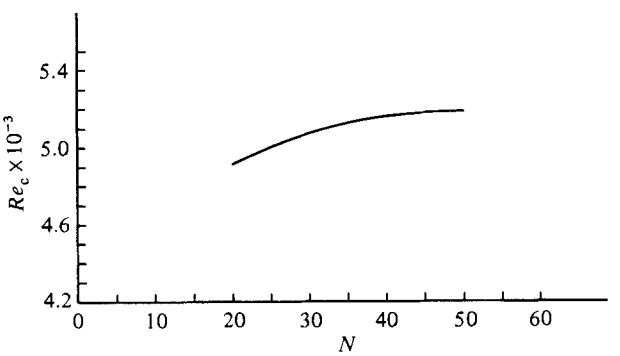

FIGURE 6. Effect of number of terms in (13); infinite disks, one disk rotating, $E^{-1} = 100$.

$\alpha_A < \alpha < \alpha_B$, Im $(c_1) < 0$ and the first eigenmode is unstable. Point $B(\alpha_B)$ is again a point of neutral stability for the first eigenmode as Im $(c_1) = 0$ here. The flow remains stable in the range $\alpha_B < \alpha < \alpha_C$. At point $C(\alpha_C)$ the eigenvalue we previously labelled c_2 becomes real, while Im (c_1) remains positive. Thus for conditions represented by point B, the second eigenvalue c_2 has become the dominant eigenvalue, and the corresponding eigenmode represents the greatest danger to flow stability. In the interval (α_C, α_D) we find Im $(c_2) < 0$, Im $(c_k) > 0, k \neq 2$, and at point D the conditions are characterized by Im $(c_2) = 0$, Im $(c_k) > 0, k \neq 2$. These conditions are clearly indicated in figure 4. Here Im $(c_k), k = 1, 2, 3$, is plotted against the arclength α. Conditions existing along contour B are shown in figure 5, where β is the arclength measured from O'.

For low dimensions of the approximating subspace the Galerkin B-spline formulation is inaccurate. Rapid convergence is found, however, on increasing N in (13), as indicated in figure 6. In this respect the reader may also consult Giron (1982). All the calculations reported in this paper were performed with $N > 40$.

The critical value of the Reynolds number from figure 2 is $Re_c = 5000$. With $E^{-1} = 100$ this places the point of instability at $r/s = 50$. For $r/s > 50$ the flow is unstable to infinitesimal disturbances.

At $E^{-1} = 275$ Holodniok *et al.* (1977) display three distinct basic flows. One of these flows, designated profile (a), is of the Batchelor type. It is a boundary-layer flow, with

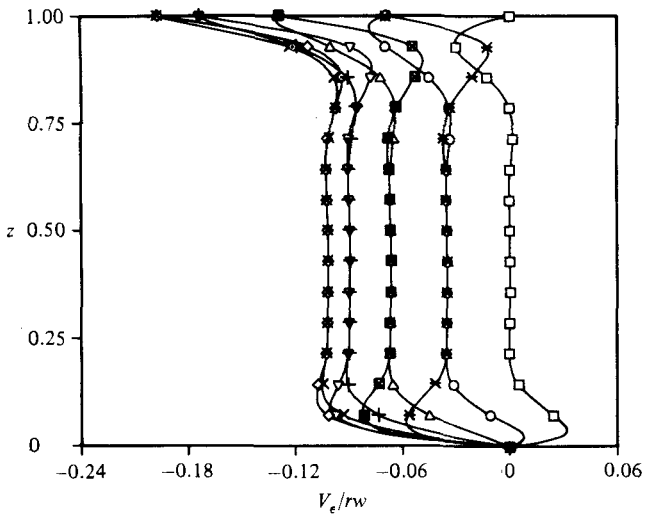

FIGURE 7. Directional behaviour of velocity (Holodniok *et al.* 1977); infinite disks, one disk rotating, $E^{-1} = 375$, profile (*a*): □, $\epsilon = 0°$; ○, 20°; △, 40°; +, 60°; ×, 80°; ◇, 100°; ▽, 120°; ⊠, 140°; *, 160°.

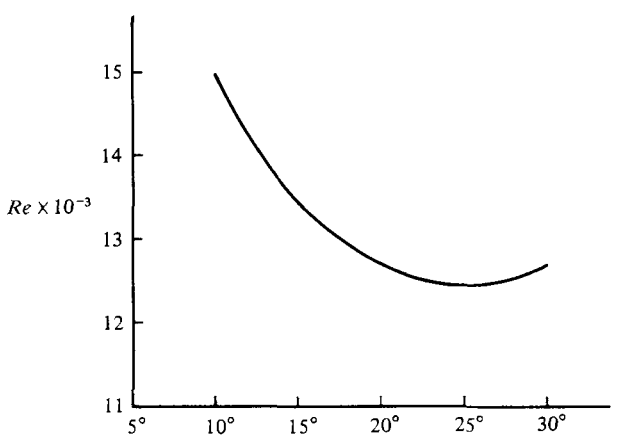

FIGURE 8. Directional behaviour of Reynolds number in marginal state; infinite disk, one disk rotating, $E^{-1} = 275$, profile (*a*).

some intermediate angular velocity in rigid-body motion. This almost-rigid core occupies approximately 60 % of the volume, leaving approximately 20 % each for the two boundary layers adjacent to the disks. Profile (*a*), which shows strong resemblance to the experimental profiles of Szeri *et al.* (1983), measured between finite disks, is projected onto the direction ϵ in figure 7. The curves of this figure show antisymmetry with respect to midchannel, and indicate that the core of the fluid moves, in any direction ϵ, with an almost uniform velocity, which is obtainable as the average of the boundary velocities at the given location and in the given direction. The flow is due primarily to the motion of the boundaries, and, at least superficially, it resembles Couette flow. The velocity distribution for $\epsilon = 25°$ appears to be the least stable; this is indicated in figure 8. This figure displays the Reynolds number, calculated at the marginal state, versus the corresponding vortex angle ϵ. The

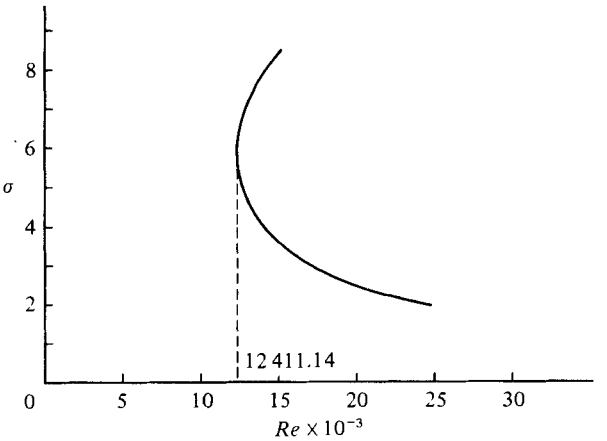

FIGURE 9. Diagram of neutral stability; infinite disks, one disk rotating, $E^{-1} = 275$, $\epsilon = 25°$, profile (a).

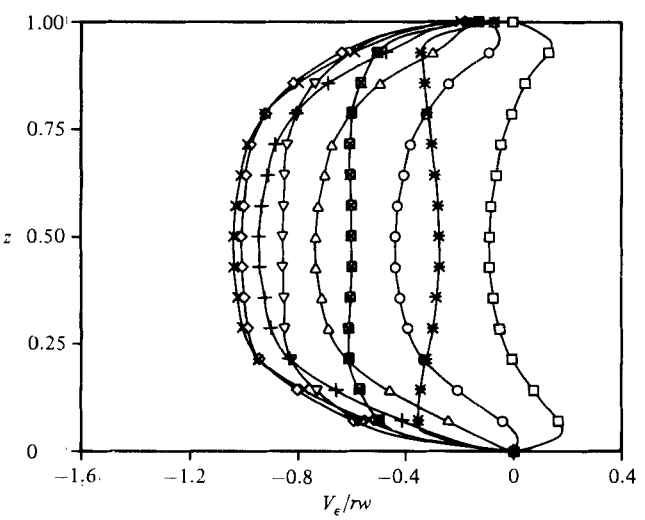

FIGURE 10. Directional behaviour of velocity (Holodniok *et al.* 1977); infinite disks, one disk rotating, $E^{-1} = 275$, profile (b): □, $\epsilon = 0°$; ○, 20°; △, 40°; +, 60°; ×, 80°; ◇, 100°; ▽, 120°; ⊠, 140°; *, 160°.

complete stability diagram is displayed in figure 9. The critical Reynolds number is $Re_c = 12411.14$. This places the point of instability at $r/s = 41.13$.

The other two solutions, profiles (b) and c), obtained by Holodniok *et al.* (1977) at $E^{-1} = 275$ are displayed in figures 10 and 11 respectively. These profiles are quite unlike profile (a), but show a great degree of similarity with one another. Both profiles (b) and (c) are symmetric with respect to midchannel. The core again moves with an almost uniform velocity. However, the core velocity may greatly exceed the velocity of either of the boundaries, and the flow resembles Poiseuille flow. Both of these profiles are found to be unstable at all values of the Reynolds number, i.e. at all positions r/s, as indicated in figures 12 and 13.

Experimental profiles of radial and tangential velocity components were obtained via laser-Doppler velocimetry in water between finite disks 50.8 cm in diameter.

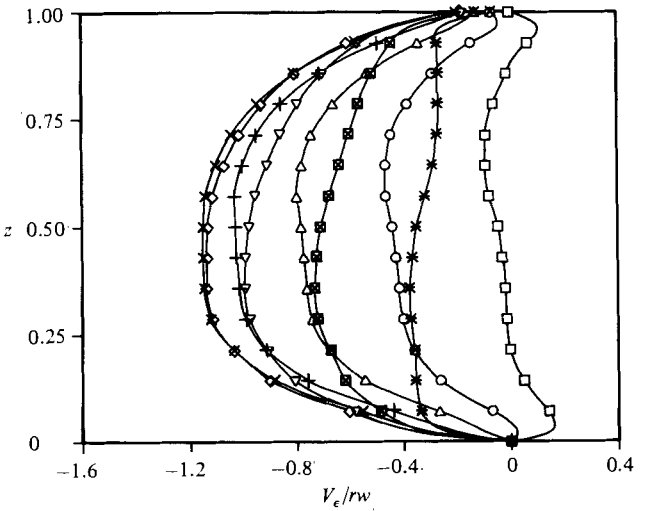

FIGURE 11. Directional behaviour of velocity (Holodniok *et al.* 1977); infinite disks, one disk rotating, $E^{-1} = 275$, profile (*c*): □, $\epsilon = 0°$; ○, 20°; △, 40°; +, 60°; ×, 80°; ◇, 100°; ▽, 120°; ⊠, 140°; *, 160°.

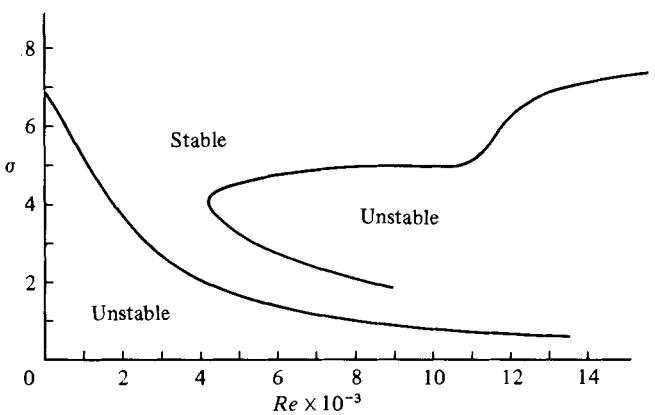

FIGURE 12. Diagram of neutral stability; infinite disks, one disk rotating, $E^{-1} = 275$, $\epsilon = 30°$, profile (*b*).

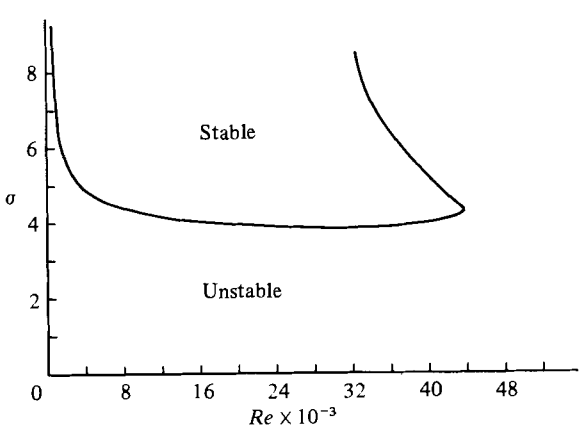

FIGURE 13. Diagram of neutral stability; infinite disks, one disk rotating, $E^{-1} = 275$, $\epsilon = 25°$, profile (*c*).

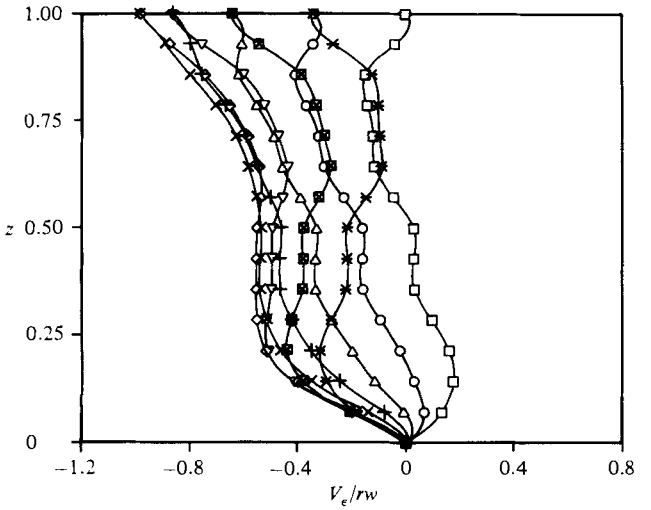

FIGURE 14. Directional behaviour of velocity; finite disks, one disk rotating, $E^{-1} = 49.98$: □, $\epsilon = 0°$; ○, 20°; △, 40°; +, 60°; ×, 80°; ◇, 100°; ▽, 120°; ⊠, 140°; *, 160°.

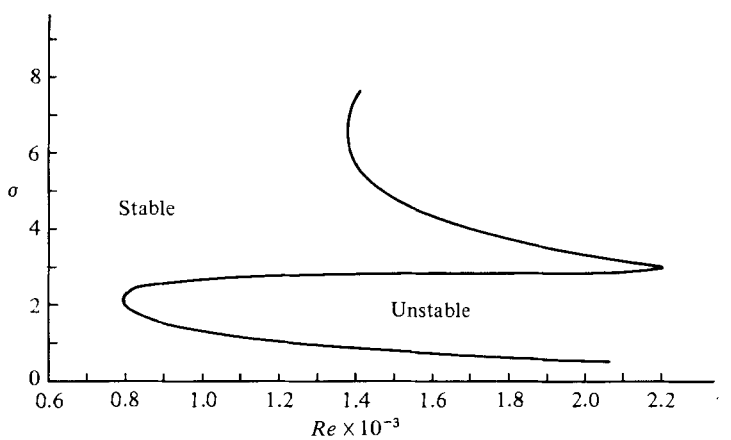

FIGURE 15. Diagram of neutral stability; finite disks, one disk rotating, $E^{-1} = 52.30$, $r/s = 14.4$, $\epsilon = 15°$.

Details of the apparatus and the measurements are given in the preceding paper (Szeri *et al.* 1983). The velocity components obtained in a gap $s = 1.26$ cm with one disk rotating and the other stationary, are combined and projected onto various directions ϵ at $r/s = 14.4$ in figure 14. To establish the position of instability for this flow we proceed as follows.

Experimental velocity profiles measured at given position r/s are analyzed for stability, as in figure 15. This figure is for $r/s = 14.4$ and shows that, had the profile remained similar for larger values for r/s, it would have become unstable at the (critical) position $(r/s)_c = 15.41$. In figure 16 we plot $(r/s)_c$ versus r/s. The position of the point of instability is given by the intersection of this curve with the $(r/s)_c = r/s$ line. Figure 16 indicates that flow between finite rotating disks, with one disk rotating and the other stationary, is least stable at the disk boundary, and in the vicinity of the axis of rotation. At midradius where the basic motion approaches the infinite-disk

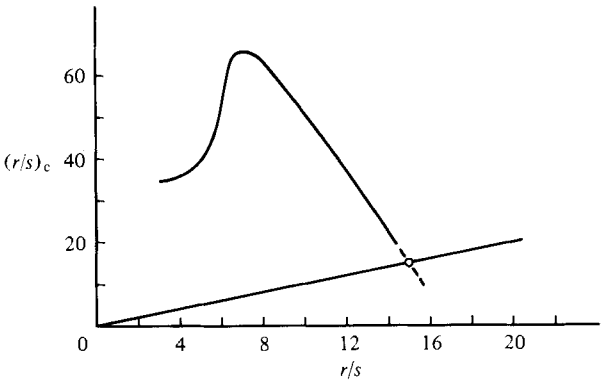

FIGURE 16. Determination of point of instability; finite disks, one disk rotating, $E^{-1} = 52.30$, $\epsilon = 15°$.

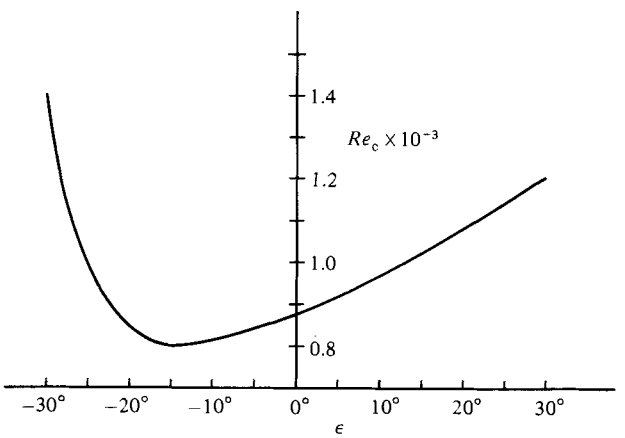

FIGURE 17. Directional dependence of Reynolds number in neutral state; finite disks, one disk rotating, $E^{-1} = 52.30$.

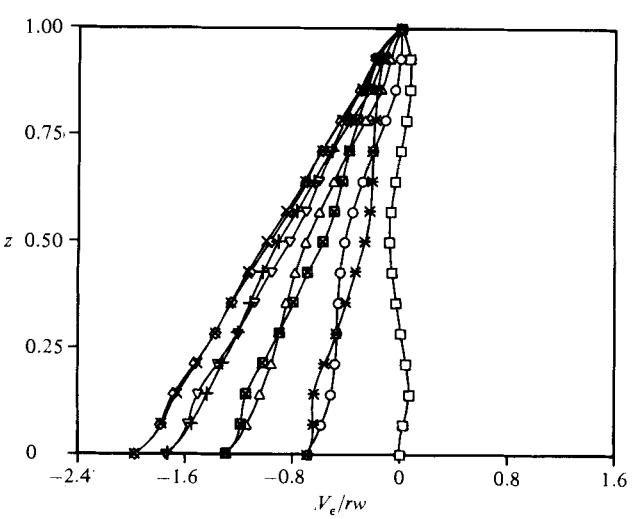

FIGURE 18. Directional behaviour of velocity; finite counter-rotating disks, $E^{-1} = 24.75$: □, $\epsilon = 0°$; ○, 20°; △, 40°; +, 60°; ×, 80°; ◇, 100°; ▽, 120°; ⊠, 140°; FT*, 160°.

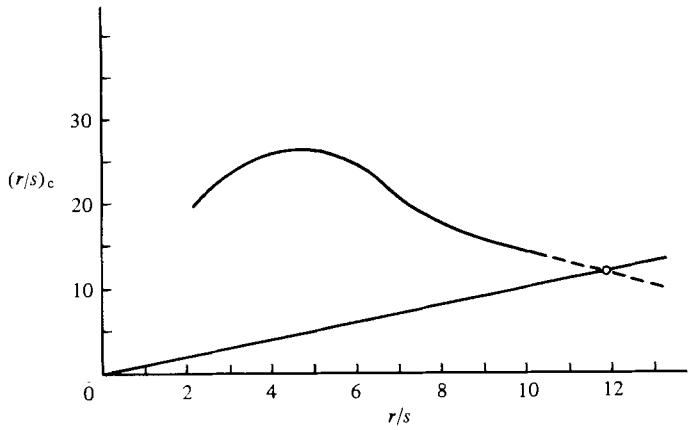

FIGURE 19. Determination of point of instability; finite counter-rotating disks, $E^{-1} = 24.75$, $\epsilon = 10°$.

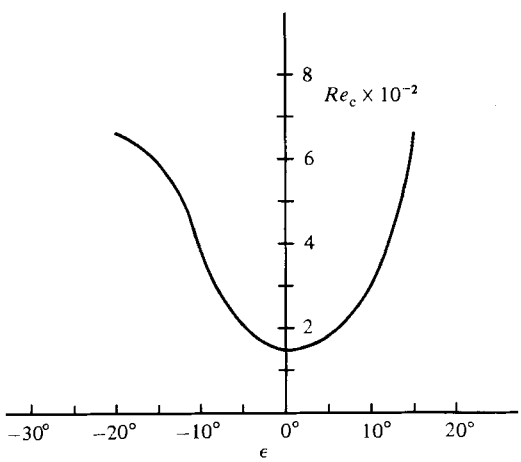

FIGURE 20. Directional behaviour of Reynolds number in neutral state; finite counter-rotating disks, $E^{-1} = 24.75$.

solution (Szeri *et al.* 1983), the stability characteristics of the finite-disk approach those for infinite-disk flow. Figure 16 yields $r/s = 15.2$ as the position of neutral stability. The critical value of the real Reynolds number is $Re = 795.0$ and the critical value of the vortex angle is $\epsilon \approx 15°$ from figure 17.

Velocity profiles, measured between counter-rotating disks and projected onto directions characterized by the local angle ϵ, are shown in figure 18. The disks have equal and opposite rotation, and the velocities are depicted at $r/s = 10.67$. The point of instability is in the $r/s = 11.50$ position, judging from figure 19. Figure 20 shows the directional behaviour of the Reynolds number in the neutral state, giving $\epsilon = 0°$ for critical conditions. Figure 21 is a diagram of neutral stability for counter-rotating disks. The result of figure 21 translates into a critical (local) Reynolds number of $Re_c = 142.77$ for counter-rotating disks.

Experimentally we are able to clearly define two types of instabilities. They both appear to be horizontal roll vortices and are located in the boundary layer of each rotating disk. The instabilities were made visible with the aid of various dyes and

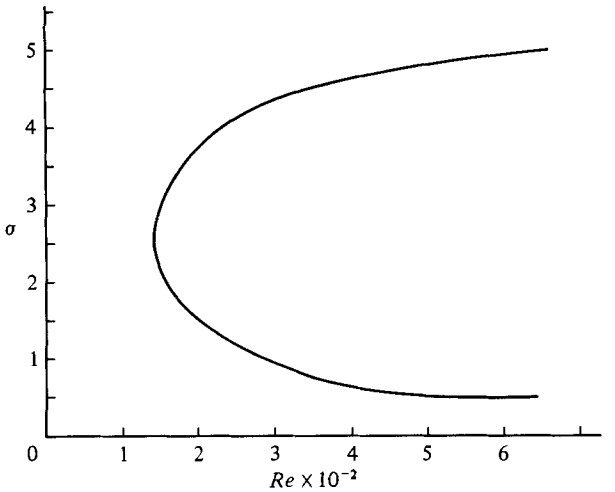

FIGURE 21. Diagram of neutral stability; finite counter-rotating disks, $E^{-1} = 24.75$, $\epsilon = 0°$.

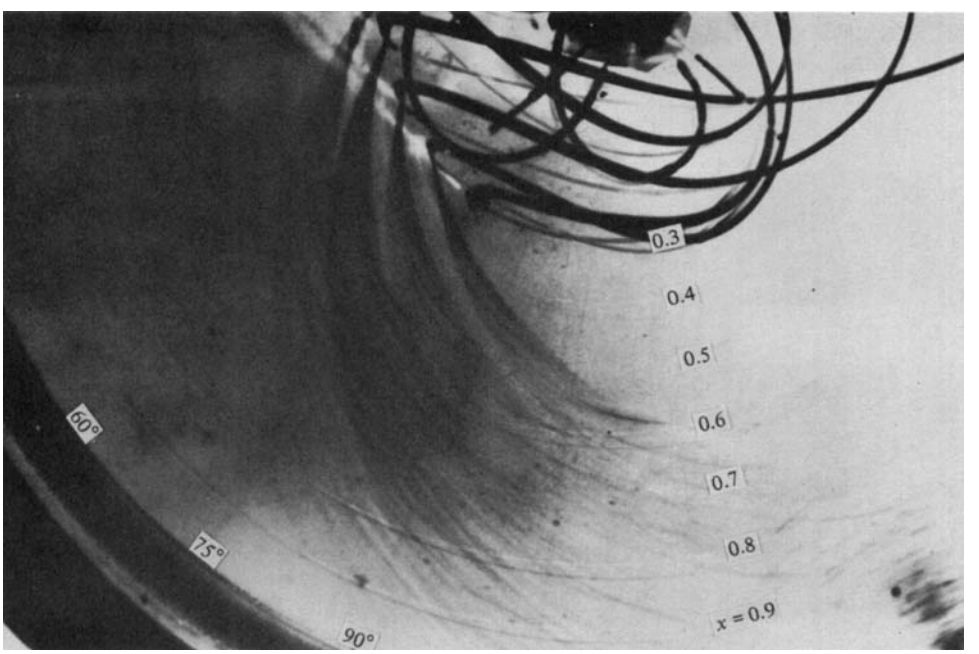

FIGURE 22. Instability between finite disks; $N_1 = 0$, $N_2 = 11.02$ rev/min.

paints. Paint was injected through hypodermic needles, mounted flush with the rotating disk and driven by a fusion pump.

One of the observed instabilities has the appearance of equiangular spirals and seems to remain stationary relative to the rotating disk. We identify this structure as the type I instability of Faller (1963). With one disk rotating and the other stationary, the spiral angle varies between 14° and 20°, with an average value of $\epsilon = 17°$. From the spacing of the vortices we estimate the number of vortices around the circumference to be $n \approx 51$. The photographs yield $r_c = 11.20$ cm for the critical radius at $N_1 = 0$, $N_2 = 11.02$ rev/min and $s = 1.26$ cm, giving $Re_T^{(1)} = 1.8 \times 10^3$ for the local Reynolds number at transition (figure 22). This structure is also observable

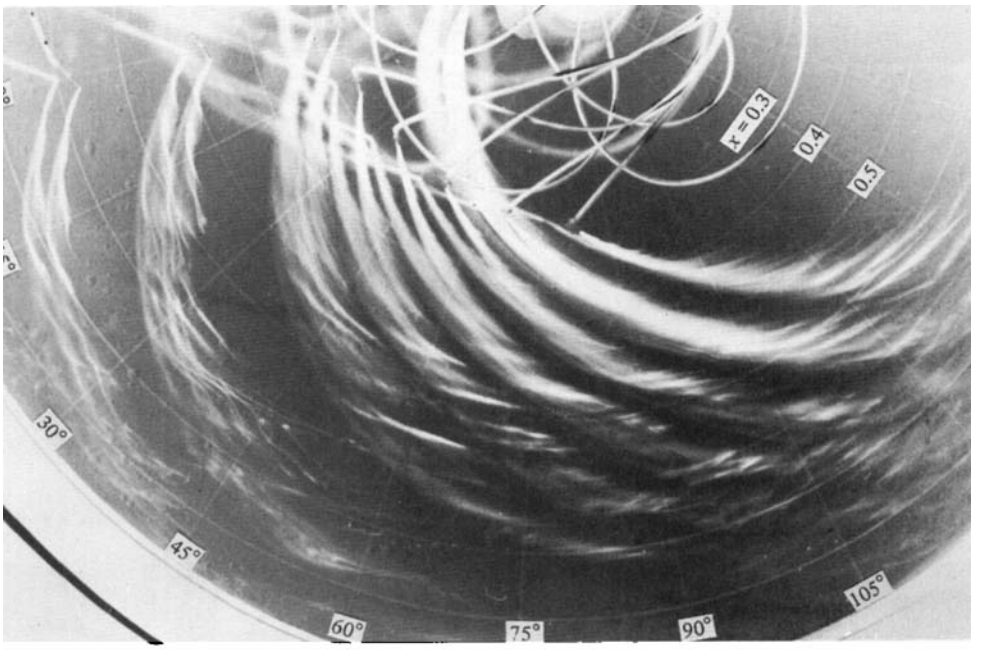

(*a*)

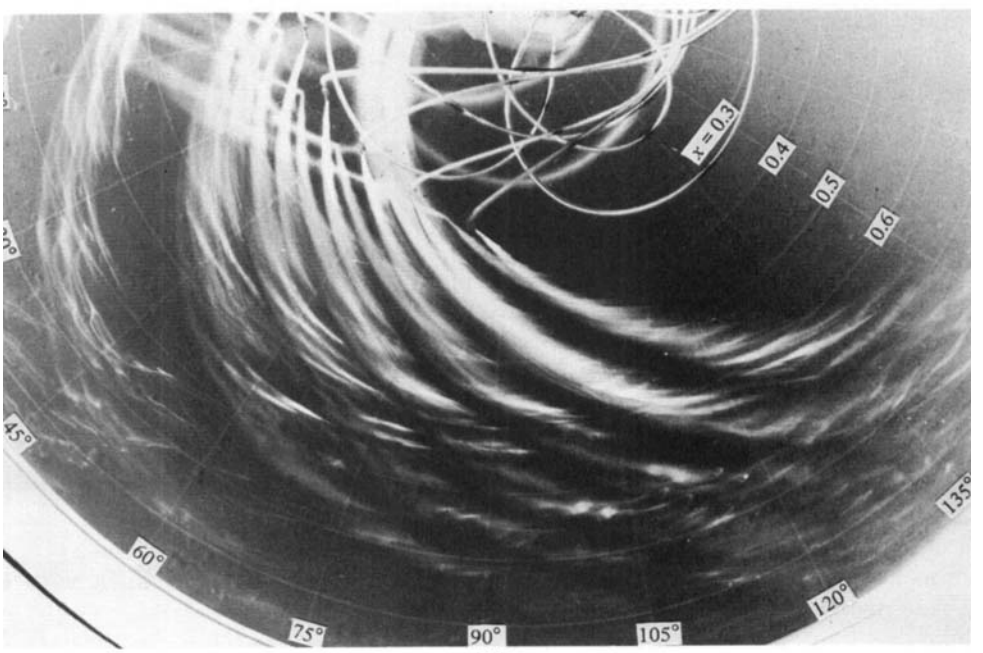

(*b*)

FIGURE 23 (*a*, *b*). For caption see facing page.

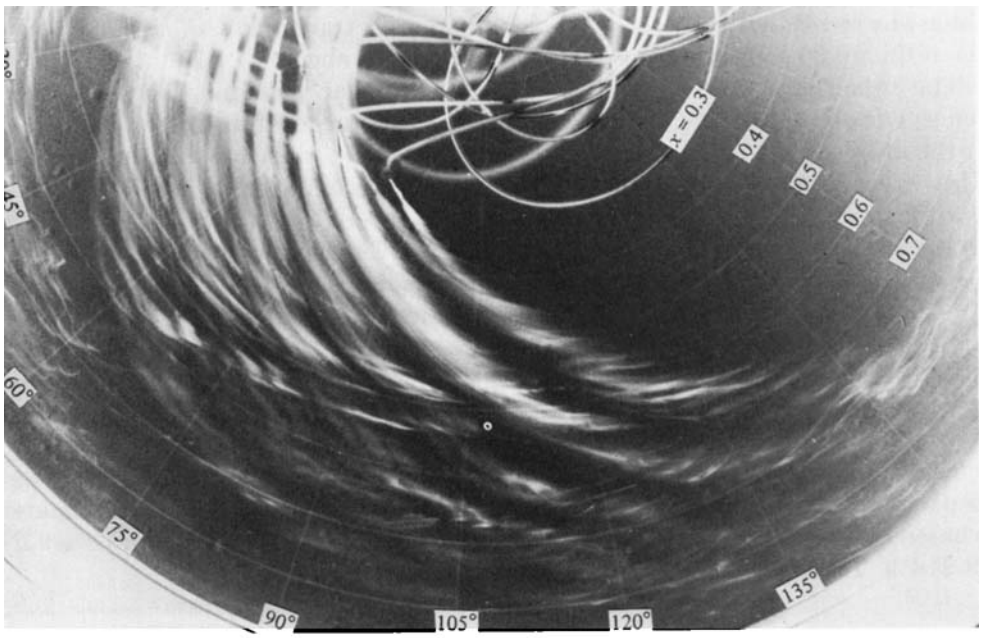

(*c*)

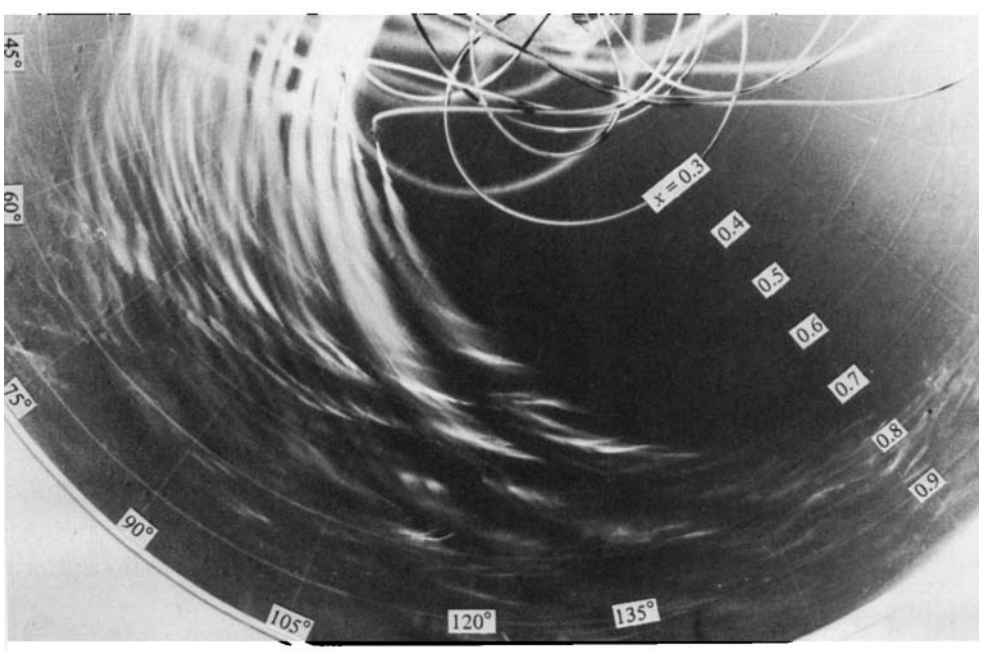

(*d*)

FIGURE 23. Instability between finite disks. Photographs taken at the rate of one frame per second, in sequence (*a*), (*b*), (*c*), (*d*) ($N_1 = -N_2 = 2.7$ rev/min).

between counter-rotating disks (figure 23), but here the vortex angle has the average value of $\epsilon = 14°$ and the local Reynolds number at transition is $Re_T^{(1)} = 5.527 \times 10^2$. We estimate 30 spirals at $N_1 = -N_2 = 2.7$ rev/min and $s = 1.26$ cm.

The other type of instability occurs in irregular patterns. The structure is concentric on the average, $\epsilon = 0°$, and between counter-rotating disks it first appears at the radius $r_c = 17.12$ cm when $N_1 = -N_2 = 2.7$ rev/min, $s = 1.26$ cm (figure 23). This gives $Re_T^{(2)} = 9.6 \times 10^2$ for the local Reynolds number at second transition. Turbulent transition is at $r = 15.94$ cm when $N_1 = -N_2 = 7.5$ rev/min, $s = 1.26$ cm, giving a local Reynolds number $Re_T^{(3)} = 1.8 \times 10^3$. The instability waves have a small velocity relative to the rotating disk in the radial direction. This is indicated in figures 23(*a–d*), which show photographs of instabilities taken at the rate of one frame per second. We identify this structure as the type II instability of Faller (1963). Although type II instability has been observed with one disk rotating and the other stationary, we were unable to obtain satisfactory photographic evidence in that case.

The authors wish to thank Mr Ching-Yue Lai of the Mechanical Engineering Department, University of Pittsburgh, for valuable assistance received. This material is based upon work supported by the National Science Foundation under Grant MEA 78-21853. This support is gratefully acknowledged.

Appendix

The Galerkin coefficients are given by B-spline inner products as follows:

$$\bar{Z}_{ijk}^{(\alpha)} = \int_0^1 B_i^{(a)}(z)\, B_j^{(b)}(z)\, B_k^{(c)}(z)\, \mathrm{d}z,$$

$$\bar{z}_{jk}^{(\alpha)} = \int_0^1 B_j^{(b)}(z)\, B_k^{(c)}(z)\, \mathrm{d}z, \quad (a \leqslant b \leqslant c),$$

$$\alpha = a+b+c+2\,(\text{if } a > 0)+1\,(\text{if } b > 0).$$

The matrices $\boldsymbol{A}, \ldots, \boldsymbol{N}$ of (21) are defined in terms of these coefficients:

$$A_{mi} = \delta\left\{\sum_{k=1}^{N}[2\cos\epsilon\, V_k(\bar{Z}_{mik}^{(1)} + \bar{Z}_{mki}^{(1)}) - \sin\epsilon\, U_k(\bar{Z}_{mki}^{(1)} + \bar{Z}_{mik}^{(1)})] - 2\bar{z}_{mi}^{(1)}\right\}$$

$$B_{mj} = \sum_{k=1}^{N}[U_k(\bar{Z}_{mkj}^{(2)} - \sigma^2\bar{Z}_{mkj}^{(0)} - \bar{Z}_{mjk}^{(2)}) + \delta^2\cos\epsilon\, W_k(\bar{Z}_{mjk}^{(1)} + \bar{Z}_{mkj}^{(0)})],$$

$$C_{ni} = \sum_{k=1}^{N}\left\{\left[\left(1 - \left(\frac{\delta}{\sigma}\right)^2(1+\sin^2\epsilon)\right)U_k + \left(\frac{\delta}{\sigma}\right)^2\sin\epsilon\cos\epsilon\, V_k\right]\bar{Z}_{nki}^{(0)} - \left(\frac{\delta}{\sigma}\right)^2 W_k\cos^2\epsilon\,\bar{Z}_{nki}^{(1)}\right\} - 2\sin\epsilon\,\bar{z}_{ni}^{(0)},$$

$$D_{nj} = \frac{\delta}{\sigma^2}\sum_{k=1}^{N}[2(V_k\cos\epsilon - U_k\sin\epsilon)\bar{Z}_{nkj}^{(1)} - V_k\cos\epsilon\,\bar{Z}_{njk}^{(1)}] - 2\bar{z}_{nj}^{(0)},$$

$$E_{mi} = \left(\frac{\delta}{\sigma}\right)^2\left\{\sum_{k=1}^{N}[V_k(1+\cos^2\epsilon) - U_k\cos\epsilon\sin\epsilon)\left(\bar{Z}_{mik}^{(1)} + \bar{Z}_{mki}^{(t)}\right) + W_k\sin\epsilon\,\bar{Z}_{mki}^{(3)}] - 2\cos\epsilon\,\bar{z}_{mi}^{(1)}\right\},$$

$$F_{mj} = -\frac{\delta}{\sigma}\sum_{k=1}^{N}\Big\{V_k \sin\epsilon\,(\overline{Z}^{(2)}_{mkj}+\overline{Z}^{(3)}_{mjk}) - W_k\,[\overline{Z}^{(4)}_{kmj}+\sigma^2\,(\overline{Z}^{(1)}_{mjk}+\overline{Z}^{(1)}_{mkj}) - \cos\epsilon\,U_k\,(\overline{Z}^{(2)}_{mjk}+2\sigma^2\,\overline{Z}^{(0)}_{mkj}-\overline{Z}^{(2)}_{mkj})\Big\} + \frac{1}{\sigma Re}(\bar{z}^{(5)}_{mj}-2\sigma^2\,\bar{z}^{(2)}_{mj}+\sigma^4\,\bar{z}^{(0)}_{mj}),$$

$$G_{ni} = -\frac{\delta}{\sigma}\sum_{k=1}^{N}[(2\cos\epsilon\,U_k+\sin\epsilon\,V_k)\,\overline{Z}^{(0)}_{nki}+W_k\,\overline{Z}^{(1)}_{nki}] + \frac{1}{\sigma Re}(\bar{z}^{(2)}_{ni}-\sigma^2\bar{z}^{(0)}_{ni}),$$

$$Q_{nj} = -\frac{1}{\sigma}\sum_{k=1}^{N} V_k\,\overline{Z}^{(1)}_{njk}, \quad H_{mi} = \delta\sin\epsilon\,\bar{z}^{(1)}_{mi},$$

$$I_{mj} = \bar{z}^{(2)}_{mj}-\sigma^2\,\bar{z}^{(0)}_{mj}, \quad J_{ni} = \bar{z}^{(0)}_{ni},$$

$$M_{mj} = \sigma\delta\cos\epsilon\,\bar{z}^{(0)}_{mj}, \quad N_{ni} = -\frac{\delta}{\sigma}\cos\epsilon\,\bar{z}^{(0)}_{ni} \quad (3\leqslant m,\ j\leqslant N-2;\ 2\leqslant n,\ i\leqslant N-1).$$

REFERENCES

ADAMS, M. L. & SZERI, A. Z. 1982 Incompressible flow between finite disks. *Trans ASME* E: *J. Appl. Mech.* **49**, 1–9.

BATCHELOR, G. K. 1951 Note on a class of solutions of the Navier–Stokes equations representing rotationally symmetric flow. *Q. J. Mech. Appl. Maths* **4**, 29.

BROWN, W. B. 1961 A stability criterion for three-dimensional laminar boundary layers. In *Boundary Layer and Flow Control* (Ed. G. V. Lachman), vol. 2, pp. 913–923. Pergamon.

CALDWELL, D. R. & VAN ATTA, C. W. 1970 Characteristics of Ekman boundary layer instabilities. *J. Fluid Mech.* **44**, 79–95.

DEBOOR, C. 1978 *A Practical Guide to Splines*. Springer.

DIJKSTRA, D. 1980 On the relation between adjacent inviscid cell type solutions to the rotating-disk equations. *J. Engrg Maths* **14**, 133–154.

FALLER, A. J. 1963 An experimental study of the instability of the laminar Ekman boundary layer. *J. Fluid Mech.* **15**, 560–576.

FALLER, A. J. & KAYLOR, R. E. 1966 Investigations of stability and transition in rotating boundary layers. In *Dynamics of Fluids and Plasmas* (ed. S. I. Pai), pp. 239–255. Academic.

GIRON, A. 1982 Local stability of rotating disk flows. Ph.D. thesis, The University of Pittsburgh.

GREENSPAN, H. P. 1968 *The Theory of Rotating Fluids*. Cambridge University Press.

GREGORY, N., STUART, J. T. & WALKER, W. S. 1955 On the stability of three dimensional boundary layers with application to the flow due to a rotating disk. *Phil. Trans. R. Soc. Lond.* **A248**, 155.

GROSCH, C. E. & SALWEN, H. 1968 The stability of steady and time-dependent plane Poiseuille flow. *J. Fluid Mech.* **34**, 177–205.

HOLODNIOK, M., KUBICEK, M. & HLAVACEK, V. 1977 Computation of the flow between two rotating coaxial disks. *J. Fluid Mech.* **81**, 680–699.

HOLODNIOK, M., KUBICEK, M. & HLAVACEK, V. 1981 Computation of the flow between two rotating coaxial disks: multiplicity of steady-state solutions. *J. Fluid Mech.* **108**, 227–240.

KÁRMÁN, T. VON 1921 Laminar und turbulente Reibung. *Z. angew. Math. Mech.* **1**, 233.

KOBAYASHI, R., KOHAMA, Y. & TAKAMADATE, C. 1980 Spiral vortices in boundary layer transition regime on a rotating disk. *Acta Mech.* **35**, 71–82.

MELLOR, G. L., CHAPPLE, P. J. & STOKES, V. K. 1968 On the flow between a rotating and a stationary disk. *J. Fluid Mech.* **31**, 95–112.

NGUYEN, N. D., RIBAULT, J. P. & FLORENT, P. 1975 Multiple solutions for flow between coaxial disks. *J. Fluid Mech.* **68**, 369–388.

ORSZAG, S. A. 1971 Accurate solution of the Orr–Sommerfeld stability equation. *J. Fluid Mech.* **50**, 689–703.

ROGERS, M. H. & LANCE, G. N. 1960 The rotationally symmetric flow of a viscous fluid in the presence of an infinite rotating disk. *J. Fluid Mech.* **7**, 617–631.

STEWARTSON, K. 1953 On the flow between two rotating co-axial disks. *Proc. Camb. Phil. Soc.* **3**, 333–341.

SCHLICHTING, H. 1979 *Boundary Layer Theory.* McGraw-Hill.

SZERI, A. Z. & GIRON, A. 1982 Stability of flow over an infinite rotating disk. (Unpublished manuscript.)

SZERI, A. Z., SCHNEIDER, S. J., LABBE, F. & KAUFMAN, H. N. 1983 Flow between rotating disks. Part 1. Basic flow. *J. Fluid Mech.* **134**, 103–131.

TATRO, P. R. & MOLLO-CHRISTENSEN, E. L. 1967 Experiments on Ekman layer stability. *J. Fluid Mech.* **28**, 531–543.

WARN-VARNAS, A., FOWTES, W. W., PIACSEK, S. & LEE, S. M. 1978 Numerical solutions and laser-Doppler measurements of spin-up. *J. Fluid Mech.* **85**, 609–639.

WEIDMAN, P. D. 1976 On the spin-up and spin-down of a rotating fluid. Part 2. Measurements and stability. *J. Fluid Mech.* **77**, 709–735.

WEIDMAN, P. D. & REDEKOPP, L. G. 1975 On the motion of a rotating fluid in the presence of an infinite rotating disk. In *Proc. 12th Biennial Fluid Dyn. Symp., Bialowicza, Poland.*

ZANDBERGEN, P. J. & DIJKSTRA, D. 1977 Non-unique solutions of the Navier–Stokes equation for the Kármán swirling flow. *J. Engng Maths* **11**, 176–188.